

GENERAL

# Analysis of influence of RF power and buffer gas pressure on sensitivity of optically pumped cesium magnetometer

To cite this article: Shi Rong-Ye and Wang Yan-Hui 2013 *Chinese Phys. B* **22** 100703

View the [article online](#) for updates and enhancements.

## Related content

- [Optimized Condition for Buffer Gas in Optical-Pumped Magnetometer Operated at Room Temperature](#)  
Ryuzo Kawabata, Kyoya Fukuda and Akihiko Kandori
- [Spin dynamics of the potassium magnetometer in spin-exchange relaxation free regime](#)  
Ji-Qing Fu, Peng-Cheng Du, Qing Zhou et al.
- [A High Sensitivity Laser-Pumped Cesium Magnetometer](#)  
Huang Kai-Kai, Li Nan and Lu Xuan-Hui

## Recent citations

- [Intrinsic transverse relaxation mechanisms of polarized alkali atoms enclosed in radio-frequency magnetometer cell](#)  
Yang-Ying Fu and Jie Yuan
- [Harmonic detection of magnetic resonance for sensitivity improvement of optical atomic magnetometers](#)  
M. Ranjbaran *et al*
- [Combined effect of light intensity and temperature on the magnetic resonance linewidth in alkali vapor cell with buffer gas](#)  
Yang Gao *et al*

# Analysis of influence of RF power and buffer gas pressure on sensitivity of optically pumped cesium magnetometer\*

Shi Rong-Ye(石荣晔)<sup>a)b)</sup> and Wang Yan-Hui(王延辉)<sup>a)b)†</sup>

<sup>a)</sup>Institute of Quantum Electronics, School of Electronics Engineering and Computer Science, Peking University, Beijing 100871, China

<sup>b)</sup>School of Software and Microelectronics, Peking University, Beijing 100871, China

(Received 14 January 2013; revised manuscript received 6 April 2013)

A further study is conducted on two factors which respectively influence the sensitivity of optically pumped cesium magnetometer (CsOPM). The influence of radio frequency (RF) power and the buffer gas pressure on the sensitivity is theoretically analyzed, and some properties are predicted. Based on the established measurement system and the visible Zeeman spectrum, not only is the real influence of these factors studied, but also, under our experimental condition, optimum parameters based on the measured curves are ascertained. The properties of these measured curves match the theoretical result very well. Our research attempts to provide theory reference to help magnetometer designers determine optimum parameters under certain conditions.

**Keywords:** optically pumped cesium magnetometer, buffer gas pressure, sensitivity

**PACS:** 07.55.Ge, 42.50.Gy, 32.70.Jz, 85.70.Sq

**DOI:** 10.1088/1674-1056/22/10/100703

## 1. Introduction

The attempt to obtain the extremely important information behind the extremely weak fluctuation of magnetic field has always been a strong factor in motivating us to explore precision measurement of these physical quantities. Several pioneers have done great research in this field, like the optical detection of magnetic resonance proposed by Bell and Bloom,<sup>[1]</sup> which makes it possible to detect such a weak fluctuation of magnetic field. In recent years, studies on ultrahigh sensitivity magnetometers, like alkali-metal magnetometer based on pumped atoms operating in a spin-exchange relaxation free regime<sup>[2]</sup> and diamond-based magnetometer using dense nitrogen-vacancy centers as magnetic sensors<sup>[3]</sup> have made much progress. On the other hand, high sensitivity magnetic sensors, like superconducting quantum interface device (SQUID) have many meaningful applications, like the measurement of electromagnetic interference on magnetocardiographic measurement<sup>[4]</sup> and the detection of brain auditory evoked magnetic field.<sup>[5]</sup> However, the optically pumped cesium magnetometer (CsOPM) is still one kind of commercial quantum magnetometer and, until recently, there have been still many research groups interested in this kind of magnetometer.<sup>[6]</sup> Whether in military magnetic field measurement or in civil magnetic field measurement, the practical optically pumped magnetometer possesses quite an important application value as well as prospect. Compared with other magnetometers, CsOPM has many obvious advantages like single strong resonance resulting from overlapped lines of Cs magnetic resonance spectrum,<sup>[7]</sup> good sensitivity in the level of

pT/Hz<sup>1/2</sup>, better applicability in airborne surveys, etc. To obtain high sensitivity, namely to improve the signal-to-noise ratio and to narrow down the line width, is an everlasting topic for researchers.

It is believed that the sensitivity of the magnetometer varies with experimental condition. For example, the influence of radio frequency (RF) power on line width was once quantitatively discussed by Smullin *et al.*<sup>[8]</sup> They also have made a profound contribution to ultrahigh sensitivity by reducing the spin-exchange rate. Ryuzo Kawabata *et al.*<sup>[9]</sup> have conducted experiments to optimize the condition for the buffer gas in laser-based CsOPM and experimental results have been discussed qualitatively.

In the present paper, a further study is conducted on two factors which can influence the sensitivity of CsOPM. First, the influence of RF power and the buffer gas pressure on the sensitivity is theoretically analyzed and some properties are predicted. Based on the established measurement system and the visible Zeeman spectrum, not only is the real influence of these factors studied, but also, under our experimental condition, optimum parameters based on the measured curves are ascertained. The properties of these measured curves match the theoretical result very well. Our research attempts to provide theory reference to help magnetometer designers determine optimum parameters under certain conditions.

Different from Smullin's work, our experiment is conducted not in the regime where the relaxation is dominated by spin-exchange collisions but in another regime where the relaxation also relates to spin-destruction collisions. On the other hand, in Kawabata *et al.*'s work<sup>[9]</sup> the influence of the

\*Project supported by the National Natural Science Foundation of China (Grant No. 11174015).

†Corresponding author. E-mail: wangyanhui@pku.edu.cn

buffer gas pressure on sensitivity mainly based on the qualitative analysis of experimental data was studied. We quantitatively analyze the influence and then verify the validity of our theoretical analysis experimentally. A more comprehensive and general theoretical study on the whole sensitivity is made in this work.

## 2. Theoretical analysis of CsOPM

General fundamentals of CsOPM from the view of quantum physics are listed as follows. CsOPM utilizes the Zeeman effect generated by external magnetic field. Light from an electrodeless Cs vapor lamp contains  $D_1$  (894 nm) and  $D_2$  (852 nm).  $D_2$  is removed by one filter.  $D_1$ , which is circularly polarized, passes through a glass cell containing Cs vapor and causes the optically pumping processes ending up with a macro magnetic moment. Figure 1 shows the pumping processes. Cs atoms absorb polarized  $D_1$  ( $\sigma^+$  for example) and perform transition of  $\Delta m_F = +1$ . Atoms in the excited-state  $6^2P_{1/2}$  then return to ground-state  $6^2S_{1/2}$  and repeat the process until they reach the magnetic-sublevel  $|F = 4, m_F = 4\rangle$ . As a result, nearly all Cs atoms are pumped to  $|F = 4, m_F = 4\rangle$  and a macro magnetic moment is produced. Because no  $\sigma^+$  is absorbed under this condition, the Cs vapor cell becomes transparent. When the RF is added through the cell and its frequency is adjusted to frequency interval of

$$|F = 4, m_F = 4\rangle - |F = 4, m_F = 3\rangle,$$

Cs atoms make transition back to sublevel  $|F = 4, m_F = 3\rangle$  and the Cs vapor absorbs most photons. Consequently, the cell becomes dim. This is called RF depolarization, and the frequency is Larmor frequency  $f_L$ . By using the relationship of  $\gamma B = f_L$ , where  $\gamma$  is magnetogyric ratio and  $B$  is external magnetic field, magnetic quantities are obtained.

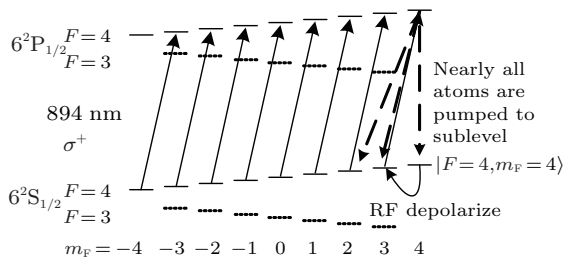


Fig. 1. Schematic diagram of optically pumped processing.

During the follow-up discussion, the relationship between the absorption of the light by the atoms and the RF field is deduced. As shown in Fig. 2, Cs light source emits  $D_1$  which is circularly polarized propagating along  $z$  axis. External magnetic field  $B_0$  is parallel to  $z$  axis. RF magnetic field lies along the  $x$  axis and passes through Cs vapor cell. Photodiode detects the variation of  $D_1$  that has passed through the cell.

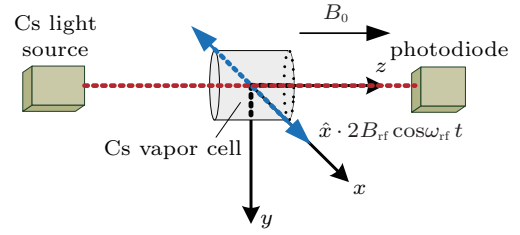


Fig. 2. (color online) Schematic diagram of system detecting the transparency of Cs vapor cell.

The intensity of light detected by photodiode is proportional to the component  $M_z$  of macromagnetic moment  $M$ . Thus, the task is converted into deducing the relationship between  $M_z$  and RF field. Equation (1) indicates the classical mechanism that electrons process around the axis of  $B_0$  at a certain angular frequency

$$\omega_0 = \gamma_{Cs} B_0. \quad (1)$$

This is Larmor frequency  $|\omega_0| = 2\pi f_L$ .  $\gamma_{Cs}$  is magnetogyric ratio of Cs. Mind that  $\gamma_{Cs}$  has negative value. According to Fig. 2, the variation of  $M$  is given by Bloch equation<sup>[10]</sup>

$$\frac{d}{dt} \begin{pmatrix} M_x \\ M_y \\ M_z \end{pmatrix} = \begin{pmatrix} M_x \\ M_y \\ M_z \end{pmatrix} \times \begin{pmatrix} \gamma_{Cs} B_{rf} \cos \omega_{rf} t \\ \gamma_{Cs} B_{rf} \sin \omega_{rf} t \\ \gamma_{Cs} B_0 \end{pmatrix} - \begin{pmatrix} \gamma_2 M_x \\ \gamma_2 M_y \\ \gamma_1 M_z \end{pmatrix} - \Gamma_P \begin{pmatrix} M_x \\ M_y \\ M_z - M_0 \end{pmatrix}. \quad (2)$$

The first term on the right-hand side of Eq. (2) is about the variation of  $M$  due to the RF field and  $B_0$ . The RF field  $\hat{x} \cdot 2B_{rf} \cos \omega_{rf} t$  can be treated as a superposition of two circularly polarized RF fields. Mind that  $B_{rf}$  is the magnitude of the RF field. Given that  $D_1$  is  $\sigma^+$ , only left rotation circularly polarized RF field plays an effective role. This is the rotating wave approximation. Taking the longitudinal relaxation and transversal relaxation into account, the rate of change of  $M$  can be described as the second term. The third term refers to the optically pumping effect.  $\gamma_2$  is the transversal relaxation rate,  $\gamma_1$  is the longitudinal relaxation rate, and  $\Gamma_P$  is the pumping rate.  $M_0$  is the macromagnetic moment resulting from the optically pumping effect. Since the optic axis is aligned with the  $z$  axis,  $M_0$  lies along the  $z$  axis.

Here, we define

$$\omega = \gamma_{Cs} B_{rf}, \quad (3)$$

and equation (2) can be solved conveniently by using coordinate transformation,<sup>[10]</sup> which leads to a steady-state solution. Then the relationship between  $M_z$  and  $\omega_{rf}$  can be described as

$$M_z = \frac{\left[ 1 + \left( \frac{\omega_0 + \omega_{rf}}{\gamma_2 + \Gamma_P} \right)^2 \right] \frac{\Gamma_P}{\gamma_1 + \Gamma_P} M_0}{1 + \frac{\omega^2}{(\gamma_1 + \Gamma_P)(\gamma_2 + \Gamma_P)} + \left( \frac{\omega_0 + \omega_{rf}}{\gamma_2 + \Gamma_P} \right)^2}. \quad (4)$$

Since  $\gamma_{\text{Cs}}$  has negative value,  $\omega_0$  and  $\omega_{\text{rf}}$  have opposite signs. Equation (4) indicates the profile of Zeeman transition spectrum, as well as its property (see Fig. 3). According to Eq. (4), when  $|\omega_0 + \omega_{\text{rf}}| = 0$ , the spectrum reaches its nadir and the expression of  $M_z$  under this condition is given in Fig. 3. On the other hand, when  $\omega_{\text{rf}}$  is far from  $\omega_0$ , we obtain  $|\omega_0 + \omega_{\text{rf}}| \gg 0$ . Then the denominator of Eq. (4) tends to  $(\omega_0 + \omega_{\text{rf}})^2(\gamma_2 + \Gamma_{\text{P}})^{-2}$ . Under this condition,  $M_z$  tends to  $\Gamma_{\text{P}}(\gamma_1 + \Gamma_{\text{P}})^{-1}M_0$ .

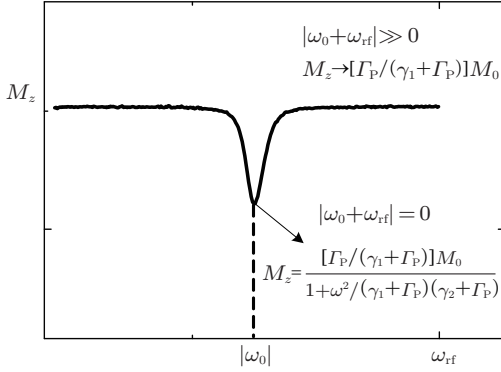


Fig. 3. Theoretical Zeeman transition spectrum.

As is well known, the intensity of light detected by photodiode is proportional to the component  $M_z$ . By using optical-to-electric signal conversion, the vertical coordinate of Fig. 3 changes to indicate voltage. On the other hand, the sensitivity of the magnetometer is defined as

$$\delta B = \frac{1}{\gamma_{\text{Cs}}} \frac{\Delta v}{S/N}, \quad (5)$$

where  $\Delta v$  is the spectral line width,  $S/N$  is the signal-to-noise ratio. In this paper,  $S/N$  means the ratio of signal peak voltage to spectral effective noise voltage in a 1-Hz band width.  $\gamma_{\text{Cs}}$  is a constant and has no contribution to the variation trend. For direct discussion, we introduce

$$\delta f = \gamma_{\text{Cs}} \cdot \delta B = \frac{\Delta v}{S/N}. \quad (6)$$

Improving signal-to-noise ratio and narrowing down the line width can make  $\delta f$  smaller. Our follow-up analyses are based on  $\delta f$  and a series of Zeeman transition spectra obtained from actual measurements.

### 3. Theoretical analysis of RF power and buffer gas pressure

#### 3.1. RF power

Now that we know much about the relationship between  $M_z$  and  $\omega_{\text{rf}}$ , it is ready for us to give a theoretical analysis to predict some properties of factors. In this paper, the spectral line width is defined as the frequency interval at half the signal peak.

Based on Fig. 3 and Eq. (4), the spectral line width can be worked out as follows:

$$\Delta f_{\text{rf}} = \frac{\Delta \omega_{\text{rf}}}{2\pi} = \frac{(\gamma_2 + \Gamma_{\text{P}})}{\pi} \left( 1 + \frac{\gamma_{\text{Cs}}^2 B_{\text{rf}}^2}{(\gamma_1 + \Gamma_{\text{P}})(\gamma_2 + \Gamma_{\text{P}})} \right)^{1/2}. \quad (7)$$

When  $B_{\text{rf}}$  satisfies  $(\gamma_1 + \Gamma_{\text{P}})^{-1}(\gamma_2 + \Gamma_{\text{P}})^{-1}(\gamma_{\text{Cs}} B_{\text{rf}})^2 \gg 1$ ,  $\Delta f_{\text{rf}}$  tends to be linear with respect to  $B_{\text{rf}}$ :

$$\Delta f_{\text{rf}} = \frac{\gamma_{\text{Cs}}}{\pi} \left( \frac{\gamma_2 + \Gamma_{\text{P}}}{\gamma_1 + \Gamma_{\text{P}}} \right)^{1/2} B_{\text{rf}}. \quad (8)$$

Equation (8) indicates the property (i) of a linear relation between the line width and  $B_{\text{rf}}$ . However, equation (8) is incomplete and correction terms should be added to the equation. Equation (8) merely describes radiation broadening which is only one of the causes. Therefore, further discussion on the causes of spectral line broadening should be taken into account.

Pressure broadening might play a partial role. Even though the buffer gas is inert, the excessively frequent and fierce collision of buffer gas particles with the Cs atom shifts its energy level, shortens the characteristic time on magnetic-sublevel  $|F = 4, m_F = 4\rangle$  and increases the uncertainty in photon absorption. This broadening effect has something to do with the buffer gas pressure  $p$ , and we treat it as  $\Delta f_{\text{b}}(p)$ . Since buffer gas is very inert,  $\Delta f_{\text{b}}(p)$  presents a tiny but observable influence.

Doppler broadening is inapplicable under our experimental condition. There is a relative motion between the Cs atoms and the RF source. The frequency received by the Cs atoms is different from the real RF frequency, which results in the broadening. According to the Lamb–Dicke criterion,<sup>[11]</sup> if the wavelength  $\lambda$  is greater than free path  $\Delta x$ , Doppler broadening can be neglected. By adding buffer gas, Doppler broadening is eliminated. The static magnetic field  $B_0$  is around 0.15 Gs (1 Gs =  $10^{-4}$  T) and the Larmor frequency is 54.1 kHz.  $c$  is light velocity and we obtain

$$\lambda = \frac{c}{2\pi f} = \frac{3 \times 10^8 \text{ m/s}}{2\pi \cdot 54.1 \text{ kHz}} = 882.56 \text{ m}. \quad (9)$$

The wavelength is far greater than the size of the cell, and we can assert that the Lamb–Dicke criterion is satisfied so long so that Doppler broadening is neglected in our analysis.

Inhomogeneous broadening could remain the same if the replaced cells are fixed at the same location of  $B_0$ . So this broadening factor is treated as constant  $\Delta f_{\text{cons}}$ . As a result, the final formula is obtained as follows:

$$\Delta f = \Delta f_{\text{cons}} + \Delta f_{\text{b}}(p) + \frac{\gamma_{\text{Cs}}}{\pi} \left( \frac{\gamma_2 + \Gamma_{\text{P}}}{\gamma_1 + \Gamma_{\text{P}}} \right)^{1/2} B_{\text{rf}}. \quad (10)$$

The intercept  $(\Delta f_{\text{cons}} + \Delta f_{\text{b}}(p))$  has a nonzero value and may grow slightly as  $p$  increases. Thus, equation (10) indicates property (ii): nonzero line width when  $B_{\text{rf}}$  tends to zero.

The next task is to deduce the formula of  $\delta f$ . Based on Fig. 3, we arrive at the formula of signal peak  $S$ :

$$S = \frac{\gamma_{\text{Cs}}^2 B_{\text{rf}}^2}{(\gamma_1 + \Gamma_{\text{P}})(\gamma_2 + \Gamma_{\text{P}}) + \gamma_{\text{Cs}}^2 B_{\text{rf}}^2} \cdot \frac{\Gamma_{\text{P}}}{\gamma_1 + \Gamma_{\text{P}}} M_0. \quad (11)$$

According to Eq. (6), we obtain  $\delta f$ :

$$\delta f = \frac{\Delta f_{\text{cons}} + \Delta f_{\text{b}}(p) + \frac{\gamma_{\text{Cs}}}{\pi} \left( \frac{\gamma_2 + \Gamma_{\text{P}}}{\gamma_1 + \Gamma_{\text{P}}} \right)^{1/2} \cdot B_{\text{rf}}}{\frac{\gamma_{\text{Cs}}^2 B_{\text{rf}}^2}{(\gamma_1 + \Gamma_{\text{P}})(\gamma_2 + \Gamma_{\text{P}}) + \gamma_{\text{Cs}}^2 B_{\text{rf}}^2} \cdot \frac{\Gamma_{\text{P}}}{\gamma_1 + \Gamma_{\text{P}}} M_0 \cdot N^{-1}}. \quad (12)$$

Equation (12) indicates the profile of  $\delta f$  which is shown in Fig. 4. For a certain cell, all quantities but  $B_{\text{rf}}$  are constant under single variable condition. Since the denominator tends to zero when  $B_{\text{rf}}$  tends to zero, there is a sharp variation before the inflection point. After the inflection point, the curve tends to perform a linear growth because  $(\gamma_1 + \Gamma_{\text{P}})^{-1}(\gamma_2 + \Gamma_{\text{P}})^{-1}(\gamma_{\text{Cs}} B_{\text{rf}})^2 \gg 1$  is satisfied. Equation (12) indicates the sharp-decreasing and slow-increasing shape of theoretical curves which we describe as property (iii). Here, we focus on the shape of the curve. By changing the parameters, the curve will be stretched, compressed or experiencing translation motion. However, the variation trend is constant and a set of parameters in Fig. 4 is chosen as an example.

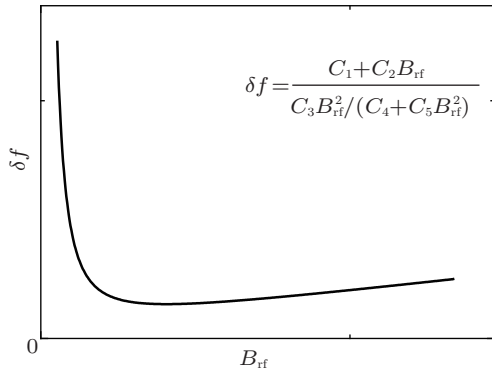


Fig. 4. Theoretical curve of  $\delta f$  where  $C_1 = C_2 = C_3 = C_4 = C_5 = 1$ .

### 3.2. Buffer gas pressure

How to manufacture Cs cell is the key technology of CsOPM. In the Cs system, there are several relaxation mechanisms working against the optical pumping processes. Wall collision during which atoms stick to the wall of the glass cell is one of the important relaxation mechanisms and the addition of an inert buffer gas in the cell is used to suppress the ballistic flight of the atoms to the walls.<sup>[12]</sup> Due to collisions with the buffer gas the alkali atom rather diffuses slowly through the gas atmosphere.<sup>[13]</sup> Therefore, how the buffer gas pressure influences the sensitivity needs to be intensively studied.

Before we display the properties of the influence of this factor, it is necessary to analyze the influence of the buffer gas

pressure on  $\gamma_2$  and  $\gamma_1$ . The pumping rate  $\Gamma_{\text{P}}$  is mainly determined by the property of pumping light, and disturbance from pressure is negligible.

The transversal relaxation rate  $\gamma_2$  is the decay rate for the component of  $M$  perpendicular to  $B_0$ , and it corresponds to a decoherence of the transverse spin magnetization of the valence electron. The collisions with the buffer gas would inevitably make the Cs atom lose its coherence with the magnetic fields (including  $B_0$  and RF field). The increase of the buffer gas pressure causes the increase of  $\gamma_2$ . However, this variety of  $\gamma_2$  fails to play a decisive role because the major part of  $\gamma_2$  refers to the spin-exchange collisions<sup>[14]</sup> of the Cs atom system and the buffer gas exerts a secondary influence.

The longitudinal relaxation rate  $\gamma_1$  involves the redistribution of the population of the Cs atom states in order to reach the Boltzmann distribution and it is partially dependent on the energy exchange with the surroundings. The collision between Cs and inert nitrogen is almost elastic. By adding the buffer gas, the chance of energy exchange within polarized Cs atoms or between Cs atoms and the wall of the glass cell is reduced. Hence,  $\gamma_1$  may rapidly decrease as the pressure increases. However, the trend will develop toward the opposite direction when the pressure becomes extreme. The excessive collisions make it inaccurate to neglect the energy exchange between Cs and nitrogen. So  $\gamma_1$  may slightly rise up in the case of extreme pressure. The analysis also corresponds to what Franzen<sup>[15]</sup> put forward:

$$\gamma_1 = C \cdot D_0 \frac{p_0}{p} + N_0 \sigma v \frac{p}{p_0}, \quad (13)$$

where  $C$  is the constant that relates to the size of vapor cell,  $D_0$  is the diffusion constant of the alkali-metal atom within the buffer gas,  $p_0$  is the standard pressure,  $p$  is the buffer gas pressure,  $v$  is the mean relative velocity of the alkali-metal atom and buffer gas atoms, and  $\sigma$  is the cross section of the alkali-metal atom in the collision with the used buffer gas. Equation (13) indicates that as  $p$  grows,  $\gamma_1$  first sharply reduces and then rises up.

According to Eq. (10), the increase rate of the spectral line width  $k_{\text{width}}$  is

$$k_{\text{width}} = \frac{\gamma_{\text{Cs}}}{\pi} \left( \frac{\gamma_2 + \Gamma_{\text{P}}}{\gamma_1 + \Gamma_{\text{P}}} \right)^{1/2}. \quad (14)$$

Here, we have the property (iv): as the pressure increases,  $\gamma_1$  decreases and  $\gamma_2$  increases. So, under higher pressure, the spectral line width increases faster. In the case of extreme pressure, the  $\gamma_1$  slightly rises up and the growth rate of the slope slows down.

For the following analysis, we write Eq. (12) in the following form:

$$\delta f = \Gamma_{\text{P}}^{-1} M_0^{-1} N \times [\pi^{-1} \gamma_{\text{Cs}} (\gamma_1 + \Gamma_{\text{P}})^{1/2} (\gamma_2 + \Gamma_{\text{P}})^{1/2} \cdot B_{\text{rf}}$$

$$\begin{aligned}
 & + (\Delta f_{\text{cons}} + \Delta f_{\text{b}}(p)) (\gamma_1 + \Gamma_{\text{P}}) \cdot B_{\text{rf}}^0 \\
 & + \pi^{-1} \gamma_{\text{Cs}}^{-1} (\gamma_1 + \Gamma_{\text{P}})^{3/2} (\gamma_2 + \Gamma_{\text{P}})^{3/2} \cdot B_{\text{rf}}^{-1} \\
 & + \gamma_{\text{Cs}}^{-2} (\Delta f_{\text{cons}} + \Delta f_{\text{b}}(p)) (\gamma_1 + \Gamma_{\text{P}}) (\gamma_2 + \Gamma_{\text{P}}) \\
 & \times B_{\text{rf}}^{-2}]. \quad (15)
 \end{aligned}$$

In this case,  $\gamma_1$  plays a decisive role. Under different pressures,  $\delta f$  curves may share a similar shape to Fig. 4. However, as can be seen in Eq. (15), their vertical position is determined by the zero-order term. Thus, when the pressure increases,  $\gamma_1$  rapidly decreases and the whole curve comes downward obviously (similar to vertical translation). In the case of extreme pressure,  $\gamma_1$  rises up slightly and the whole curve begins to go upward slowly. Thus, property (v) is obtained. The lower the curve and its inflection point, the better the sensitivity will be.

#### 4. Experimental apparatus

Figure 5 shows the experimental apparatus.  $D_1$  from the Cs discharge lamp is circularly polarized. The normal power consumption and optical power of the lamp are 2 W and 2 mW respectively. The collimated beam diameter is 14 mm. Photodiode detects the intensity of  $D_1$  that has passed through the cylindrical cell (25 mm in diameter and 25 mm long) and produces photocurrent which is converted into voltage via amplifier. A signal generator provides an RF field via RF-coils and regulates frequency sweep range, interval and RF amplitude. In order to reduce the influence of outer magnetic field, the cell is surrounded by magnetic shields. The controllable static magnetic field is generated by inner coil. The whole system is put in a light-proof temperature control box to maintain a temperature of 40 °C and avoid optical interference. The data

acquisition records RF frequency and voltage simultaneously. The apparatus is 17 cm × 6 cm × 6 cm in size.

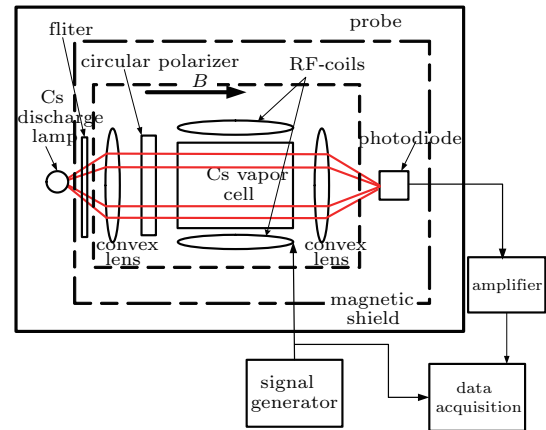


Fig. 5. (color online) Schematic diagram of the experimental apparatus.

#### 5. Experiment and results

##### 5.1. RF power

We firstly study the influence of RF power on line width and  $\delta f$  which is the counterpart of the sensitivity. A Cs vapor cell which contains about 10-kPa nitrogen is chosen as the buffer gas. Frequency sweep range is from 48 kHz to 60 kHz. Frequency sweep time is 5 s. RF power is linearly related to  $B_{\text{rf}}^2$ . In our system, the RF magnetic amplitude  $B_{\text{rf}}$  is in direct proportion to the AC amplitude controlled by the signal generator. So we define the peak-to-peak voltage of the AC output as relative RF amplitude to replace  $B_{\text{rf}}$ . As  $B_{\text{rf}}$  increases, the measured Zeeman transition spectrum varies as shown in Fig. 6.

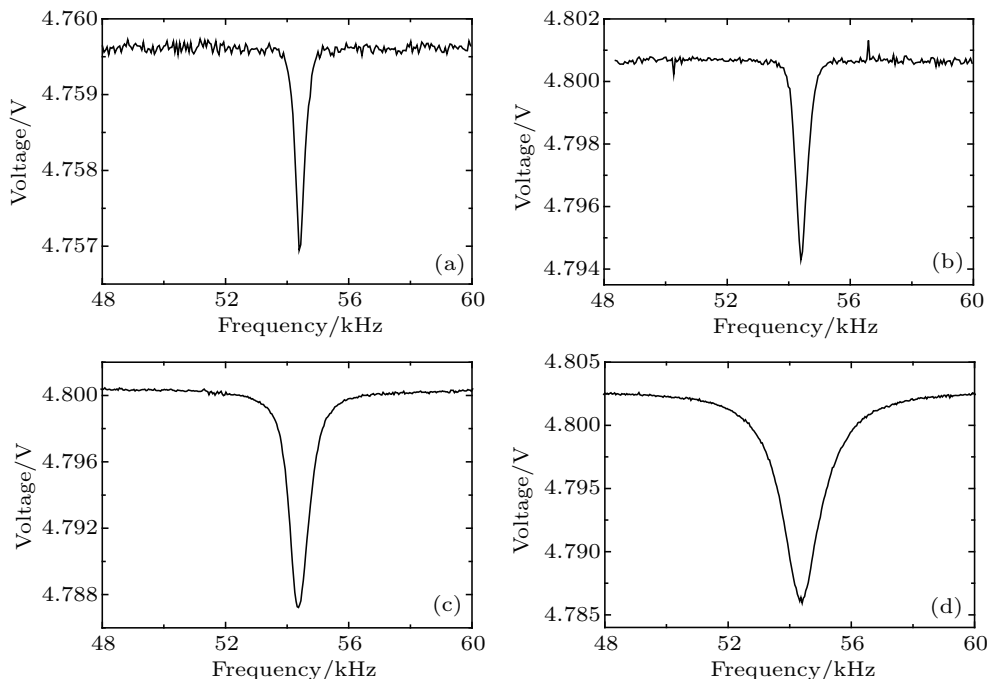


Fig. 6. Figures of Zeeman transition spectra under relative RF amplitudes of (a) 0.01 V, (b) 0.02 V, (c) 0.07 V, and (d) 0.20 V.

It can be inferred from Fig. 6 that there is an upward trend in spectral line width and  $S/N$  as relative RF amplitude increases.  $f_L$  is about 54.3 kHz. The signal peak voltage varies from 2.63 mV in a relative RF amplitude of 0.01 V to 16.50 mV in a relative RF amplitude of 0.20 V. Noise voltage presents a tiny fluctuation.

The data are further processed to observe the line width and  $\delta f$  respectively. As figure 7 shows, the spectral line width rises as the relative RF amplitude increases. The curve indicates a seemingly linear relation between the two. The phenomenon is repeatable. Linear fitting is done and the intercept is around 0.20 kHz.

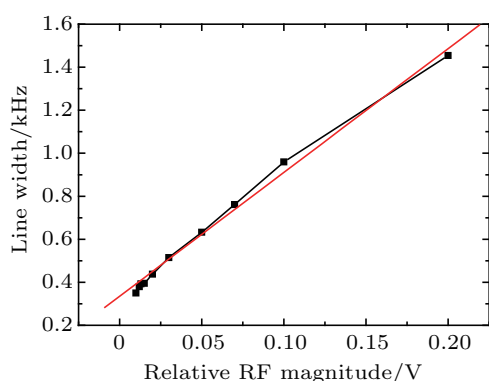


Fig. 7. (color online) Line width rising as the relative RF amplitude increases.

On the other hand, as figure 8 shows,  $\delta f$  falls sharply before 0.05 V and then keeps rising slowly as the relative RF amplitude continues to increase. The nadir of curve corresponds to the best  $\delta f$ . In other words, the relative RF amplitude of 0.05 V corresponds to the optimal RF power under a particular experimental condition.

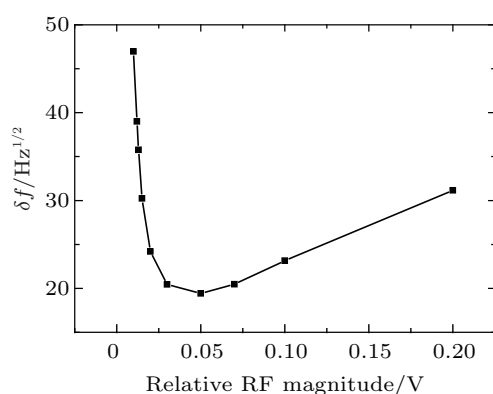


Fig. 8. Curve of  $\delta f$  versus relative RF field magnitude.

Here, several phenomena have been observed: i) a seemingly linear relation between the line width and  $B_{rf}$ , ii) nonzero line width when  $B_{rf}$  tends to zero, and iii) the sensitivity curve with a sharp-decreasing and slow-increasing shape. These phenomena respectively match the theoretical properties mentioned above which help us determine the optimal RF power.

## 5.2. Buffer gas pressure

$N_2$  is used as the buffer gas and the pressures are 1 kPa, 2 kPa, 5 kPa, 10 kPa, 15 kPa, 20 kPa. The shape and size of the cells are the same as those mentioned above. During experiments of the buffer pressure, any other factors are kept unchanged to ensure single variable condition.

Figure 9 shows the fitting lines of the line width under different buffer gas pressures. As the pressures increase, the slope of the line grows obviously. But under higher pressure conditions like 15 kPa and 20 kPa, the growth rate of the slope slows down. Each intercept has a nonzero value and increases slightly.

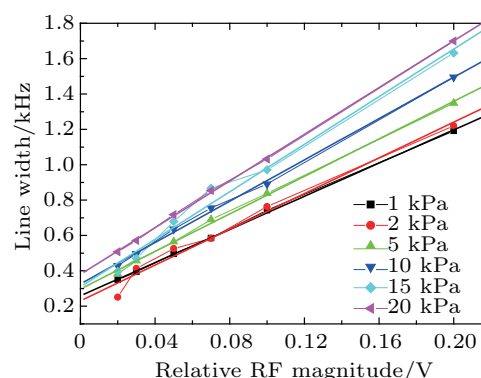


Fig. 9. (color online) Fitting lines of the line width under different buffer gas pressures.

Figure 10 shows the curves of  $\delta f$  versus relative RF field magnitude under different buffer gas pressures. These curves have similar shapes. The variation trend is that the whole  $\delta f$  curve falls before 10 kPa and then goes up slowly as the pressure continues to increase. The lower the curve, the better the sensitivity will be. Since the lowest curve corresponds to 10 kPa, 10 kPa is determined as the optimal buffer gas pressure under our experiment condition.

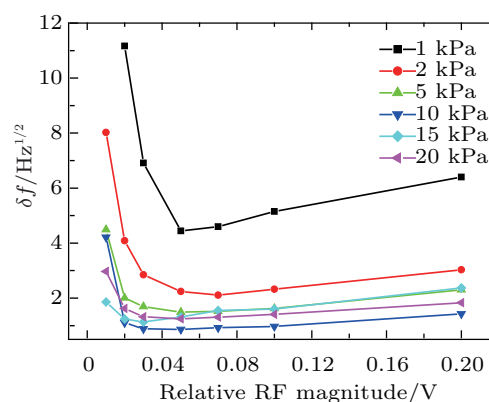


Fig. 10. (color online) Curves of  $\delta f$  versus relative RF field magnitude under different buffer gas pressures.

Here, two more phenomena are observed. iv) Under higher pressure, the spectral line width increases faster along with the increase of  $B_{rf}$  and the growth rate of the slope slows

down under extreme pressure. v) The vertical position of each whole  $\delta f$  curve has a sharp-decreasing and slow-increasing variation trend as the pressure increases. These real properties also respectively match the theoretical properties mentioned above. Based on them, the optimal buffer gas pressure can be determined. Accordingly, based on Eq. (5), the best sensitivity is estimated to be  $39.2 \text{ pT/Hz}^{1/2}$ .

So far, the correspondence has been established between theoretical analysis and experimental results. On the other hand, the experimental data provided by Kawabata *et al.*<sup>[9]</sup> are essentially consistent with ours. Thus, the validity of the theoretical result has been supported from several aspects.

## 6. Conclusion

In this paper, further theoretical analyses on the influence of RF power and the buffer gas pressure on the sensitivity have been respectively made and some predicted properties of the factors are provided. By establishing a lamp-based optically pumped cesium magnetometer experimental system, optimum parameters are ascertained based on the measured curves. The deduced equations greatly match the experimental results. Our

research can be regarded as a theory reference when magnetometer designers determine optimum parameters under certain conditions.

## References

- [1] Bell W E and Bloom A L 1957 *Phys. Rev.* **107** 1559
- [2] Dang H B, Maloof A C and Romalis M V 2010 *Appl. Phys. Lett.* **97** 151110
- [3] Taylor J M, Cappellaro P, Childress L, Jiang L, Budker D, Hemmer P R, Yacoby A, Walsworth R and Lukin M D 2008 *Nat. Phys.* **4** 810
- [4] Gu H F, Cai W Y, Wei Y K, Liu Z H, Wang Q, Wang Y, Dai Y D and Ma P 2012 *Chin. Phys. B* **21** 040702
- [5] Zhang S L, Liu Y B, Zeng J, Wang Y L, Kong X Y and Xie X M 2012 *Acta Phys. Sin.* **61** 020701 (in Chinese)
- [6] Huang K K, Li N and Lu X H 2012 *Chin. Phys. Lett.* **29** 100701
- [7] Alexandrov E B 2003 *Phys. Scr.* **2003** 27
- [8] Smullin S J, Savukov I M, Vasilakis G, Ghosh R K and Romalis M V 2009 *Phys. Rev. A* **80** 033420
- [9] Kawabata R, Fukuda K and Kandori A 2010 *Jpn. J. Appl. Phys.* **49** 082401
- [10] Bloch F 1946 *Phys. Rev.* **70** 460
- [11] Dicke R H 1953 *Phys. Rev.* **89** 472
- [12] Bison G 2004 "Development of an Optical Cardio-magnetometer", Ph. D. Thesis (Freiburg: University of Freiburg)
- [13] Dehmelt H G 1957 *Phys. Rev.* **105** 1487
- [14] Ledbetter M P, Savukov I M, Acosta V M, Budker D and Romalis M V 2008 *Phys. Rev. A* **77** 033408
- [15] Franzen W 1959 *Phys. Rev.* **115** 850